ORIGINAL PAPER

Eco-friendly synthesis and antibacterial potential of chitosan crosslinked-EDTA silver nanocomposite (CCESN)

S. A. Atanda[1,2]* , R. O. Shaibu[1] and F. O. Agunbiade[1]

Abstract

This study presents a novel and eco-friendly approach for synthesizing silver nanocomposite at room temperature. The method utilizes chitosan derived from snail (*Archachatina marginata*) shell waste crosslinked with EDTA as a combined reducing and capping agent. The existence of silver nanoparticles in the composite was confirmed by transmission electron microscopy (TEM), scanning electron microscopy (SEM), X-ray diffractometry (XRD), energy dispersive X-ray (EDX), energy dispersive X-ray fluorescence (EDXRF) and thermogravimetric analysis (TGA). The TEM, SEM, XRD, and analyses revealed that the silver nanoparticle has a face-centered cubic structure with an average size of 45.30 nm respectively. EDX and EDXRF showed characteristic silver peaks confirming the formation of silver nanoparticles in the composite while TGA indicated that silver nanoparticles contributed to good thermal stability of the composite. The formation of silver nanoparticles was indicated by a brown color transformation and an ultraviolet visible (UV Vis) absorption peak at 435 nm. The synthesized nanocomposite demonstrated promising antibacterial activity against both *Staphylococcus saprophyticus* DSM 18669 and *Escherichia coli* O157 strains, with *S. saprophyticus* showing higher susceptibility. This highlights the potential of chitosan-EDTA silver nanocomposites as alternative antimicrobial agents.

Keywords Silver nanocomposite, Antimicrobial resistance, Nanoparticle, Face-centered cubical, Gram-positive, Gram-negative

Introduction

Nanotechnology deals with the manipulation of materials at the nanometer scale, with potential applications across various fields like consumer products, biomaterials, and energy generation (Verstraete et al. 2009; Hajialyan et al. 2018; Tahvilian et al. 2019).

Several methods exist for nanoparticle production, including chemical, physical, and biological approaches (Khwannimit et al. 2019). The chemical approach offers a rapid synthesis of large quantities but necessitates capping agents to control particle size (Dhaka et al. 2023). However, this method often relies on hazardous chemicals and generates environmentally unfriendly byproducts.

Consequently, there is a growing interest in developing biological synthesis strategies that minimize reliance on toxic substances, aiming for an eco-friendly approach to nanoparticle production. This rising demand for sustainable solutions has fuelled the development of "green nanotechnology" (Krithiga et al. 2015).

Baran and colleagues (2023) asserted that the escalation of antibiotic resistance in bacteria, attributed to either extensive utilization or improper dispensation, is perceived as an indicator of the prospective redundancy of presently predominant antibiotics. Silver's

*Correspondence:
S. A. Atanda
the19icon@gmail.com
[1] Present Address: Department of Chemistry, University of Lagos, Akoka, Nigeria
[2] Nigerian Stored Products Research Institute, Ilorin, Nigeria

Atanda *et al. J Mater. Sci: Mater Eng.* (2024) 19:22

Page 2 of 17

antimicrobial activity is well-established and it functions as a potent antibacterial agent; nevertheless, the precise mechanism and mode of action remain ambiguous (Sharma and Yngard 2009). Silver nanoparticles exhibit high antibacterial activity due to their high surface-to-volume ratio, which facilitates maximum contact with the environment (Krutyakov et al. 2008). The high surface area of nanosilver is a crucial factor in its exceptional antimicrobial activity. With a larger surface area, nanosilver has more contact points with microorganisms, facilitating the transfer of silver ions and amplifying the antimicrobial effect (Liu et al. 2020a, b). This increased surface area also enables the release of more silver ions, which are responsible for the antimicrobial activity (Hadrup and Lam 2019). Furthermore, the high surface area of nanosilver allows it to penetrate deeper into biofilms, reaching and killing more microorganisms (Kvitek et al. 2019). The high surface energy of nanosilver also increases its reactivity, enabling it to more efficiently interact with and damage microbial cell membranes (Liu et al. 2020a, b). In summary, the high surface area of nanosilver is a key contributor to its high antimicrobial activity, enabling increased interaction with microorganisms, enhanced release of silver ions, improved penetration into biofilms, and increased reactivity. It is vital to manage and observe silver nanoparticles' size, shape, and stability in such applications (Kaviya et al. 2011).

Chitosan, a linear polysaccharide, is found in the shells of crustaceans and mollusks. It is formed through the process of deacetylation of chitin (Mohammed et al. 2017). Chitosan is used in biomedicine due to its biocompatibility, low allergenicity, biodegradability, and nontoxicity (Wang et al. 2020; Wei et al. 2020). The extensive applications of chitosan in textiles, cosmetics, water treatment, and food processing industries have continued to garner significant interest (Rinaudo 2006). The presence of numerous primary amino groups enhances its hydrophilic properties, allowing it to interact effectively with nanoparticles, polymers, cells, and drugs in aqueous solutions as binders and stabilizers (Almalik et al. 2017; Mirzazadeh, et al. 2020).

Chitosan and nanosilver are both known for their antimicrobial properties, but the nano nature of silver can be an added superiority over chitosan in several ways. Chitosan exhibits antimicrobial activity against a wide range of bacteria, fungi, and viruses (Kumar et al. 2020), works by disrupting cell membranes, inhibiting protein synthesis, and activating immune responses (Sarwar et al. 2020), and is generally considered safe and biocompatible (Kumar et al. 2020).

In contrast, nano-sized silver particles have a larger surface area-to-volume ratio, allowing for more efficient interaction with microorganisms and enhanced

antimicrobial activity (Liu et al. 2020a, b). Additionally, nanosilver can penetrate deeper into biofilms and cellular structures, making it more effective against stubborn infections (Kvitek et al. 2019). Its high surface energy and reactivity enable it to release silver ions more efficiently, amplifying its antimicrobial effects (Hadrup and Lam 2019).

Nanosilver can also be designed to target specific microorganisms or sites of infection, reducing harm to beneficial microflora and host tissues (Kumar et al. 2020). Combining nanosilver with other antimicrobial agents, like chitosan, may produce synergistic effects, leading to enhanced efficacy and reduced development of resistance (Khan et al. 2019). Furthermore, nanosilver can be stabilized and functionalized to maintain its antimicrobial activity over time, even in harsh environments (Sarwar et al. 2020). Its multimodal mechanisms of action, including membrane disruption, protein inhibition, and DNA damage, make it more difficult for microorganisms to develop resistance (Liu et al. 2020a, b).

However, it is essential to consider the potential risks and challenges associated with nanosilver, such as toxicity to human cells and the environment, the potential for bioaccumulation and environmental persistence, and the need for careful design, synthesis, and functionalization to ensure safety and efficacy.

Green synthesis methods utilize various biomolecules like vitamins, yeasts, and plant components for nanoparticle production (Baran et al. 2021; Atalar et al. 2022). Ethylenediaminetetraacetic acid (EDTA), with its metal-binding abilities through carboxylic acid and amine groups, acts as a suitable crosslinker for chitosan. This crosslinking between functional groups in chitosan and EDTA leads to a stable, crosslinked polyelectrolyte complex structure. The addition of EDTA enhances the adsorption capacity of the complex and improves its stability in acidic environments (Putria et al. 2019; Costa et al. 2020). The addition of EDTA (ethylenediaminetetraacetic acid) significantly enhances the adsorption capacity of metal complexes, such as chitosan-EDTA-silver. EDTA forms stable chelates with metal ions, preventing precipitation and increasing their availability for adsorption (Liu et al. 2020a, b). Additionally, EDTA improves metal ion solubility, leading to higher concentrations for interaction with chitosan (Chen et al. 2019). By introducing new functional groups, EDTA modifies chitosan's surface, creating more binding sites for metal ions (Ali and Gupta 2006). Furthermore, EDTA reduces competition for adsorption sites, enhancing metal ion uptake by chitosan-based adsorbents (Tufekci and Guzel 2017).

These crosslinked chitosan-EDTA systems possess potential applications due to their photoluminescence

Atanda *et al. J Mater. Sci: Mater Eng.*   (2024) 19:22

Page 3 of 17
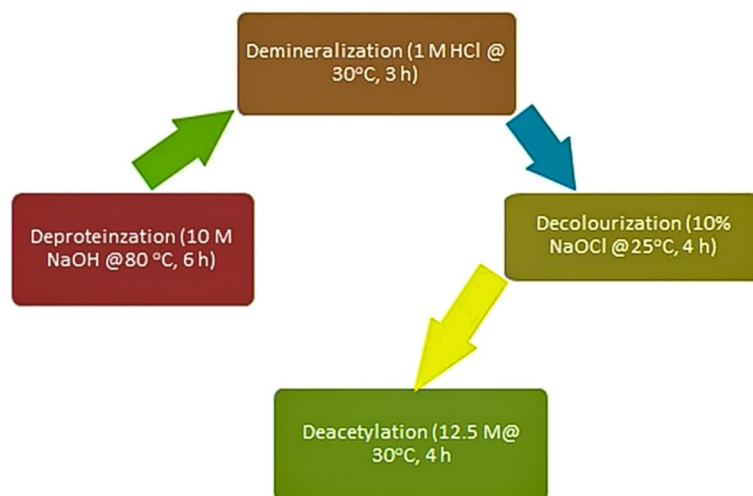
Scheme 1 Synthesis of chitosan from the shells of *Archachatina marginata*

properties (Sayaka and Nobuo 2016) and have been explored for heavy metal removal by flocculation (Verma et al. 2022). Additionally, EDTA-linked chitosan (ED-ch) demonstrates strong chelating ability and water solubility, making it valuable for biomedical applications, such as drug delivery systems that overcome the limitations of native chitosan (Verma et al. 2022).

Chitosan-silver nanocomposites exhibit dual functionality, serving as both biosensors and potential cancer treatment agents. The specificity of chitosan to cancer cells enhances its effectiveness in cancer treatment (Govindan et al. 2012). Additionally, the nanocomposite demonstrates strong antimicrobial properties and biosensing capabilities (Sanpui et al. 2008). To the best of our knowledge, this is the first report on the use of chitosan from *Archachatina marginata* shells in combination with ethylenediaminetetracetic acid (EDTA) as both a capping and reducing agent in the formation of silver nanoparticles (Almalah et al. 2019; Marambio-Jones and Hoek 2010). This study's main objectives were to synthesize chitosan-modified EDTA silver nanocomposite, characterize the nanocomposite, and evaluate its antibacterial activity against clinical strains of *Staphylococcus saprophyticus* DSM 18669 and *Escherichia coli* 0157.

Materials and methods
Synthesis of chitosan
Chitosan was extracted from the shells of *A. marginata* as shown in Scheme 1 (Oyekunle and Omoleye 2019).

Preparation of chitosan crosslinked EDTA
A 100 mL solution of acetic acid (1% v/v) and 1 g of chitosan was continuously agitated on a magnetic stirrer till complete dissolution was achieved. Thereafter,

0.34 g of EDTA was introduced to the chitosan solution in a 250-mL beaker and was stirred at 70 °C for 1 h 30 min. After that, the reaction mixture was vigorously stirred with 32 mL of ethanol until the clear solution turned opalescent. Centrifugation was used to purify the sample, and it was then re-dispersed into an ethanol solution and filtered (40% v/v) (Lin et al. 2011).

Preparation of chitosan crosslinked- EDTA- silver nanocomposite (CCESN)
Fifty milliliters of chitosan-EDTA suspension (0.001%) and 1.0 mL of $AgNO_3$ solution (5 mM) were added to a 250-mL flask to form chitosan-linked EDTA-silver nanocomposite (CCESN). For ten minutes at 25 ± 2 °C, the flask's contents were continuously swirled. The mixture was maintained at 25 °C for 10 min under uniform agitation. This was followed by a dropwise addition of 0.1 M NaOH solution to keep the solution at 10. The reaction mixture passed through gradual color transition from off-white to light brown, then to a darker shade that remained unchanged indicating the end of the reaction after 5 h. The content was allowed to cool followed by filtration and drying processes (Lin et al. 2011).

Characterization of the CCESN
Ultraviolet–visible spectrometry
Shimadzu UV-1900 UV Vis Spectrophotometer was used to perform UV–Vis spectrophotometry in the 190–1100 nm wavelength range (Rana et al. 2023). The reduction of silver ions into silver atoms (zerovalent state) was monitored via measurement of the absorbance of aliquots of the reaction mixture as the reaction progressed (Rajeshkumar and Santhiyaa 2018).

Atanda *et al. J Mater. Sci: Mater Eng.*   (2024) 19:22

Page 4 of 17

Transmission electron microscopy

Tecnai G2 Spirit TWIN FEI, Netherlands LaB6 microscope was used to investigate the morphology and distribution of the synthesized CCESN (Martin et al. 2010; de Marco et al. 2023). A small amount of the synthesized nanocomposite was placed on a carbon-coated copper grid, left to dry, and analyzed (Li 2024).

Scanning electron microscopy

Scanning electron microscopy (SEM) was used to analyze cellular morphology, size, and shape. The Phenom-World PRO:X 800–07334 scanning microscope from Thermo Fisher Scientific Company in Switzerland, serial number MVE01570775, was utilized for the SEM examination. The sputter coater was used to provide a 25-nm gold coating to an aluminum stub that held the sample at 25 mm in diameter. The sample then adhered to the carbon disc. The samples were then scanned using a 5-kV accelerating voltage and a backscattered electron detector with a focussed fine stream of secondary electrons.

X-ray diffractometry

An ARL'XTRA diffractometer from Thermo Fisher Scientific Company Switzerland was used to obtain the orientation and phase of the nanocomposite. Measurements were performed in the 2θ range from 10° to 70°, utilizing Cu Kα radiation with a wavelength (λ) of 1.5406 Å and a Nickel monochromator. The diffractometer was operated at 40 kV and a current of 30 mA (Kaur et al. 2023). A small portion of the synthesized CCESN was placed in a sample holder and inserted into the equipment giving diffraction patterns. Scherer's equation was used to calculate the average size of the crystallites in the nanocomposite (Kaviya et al. 2011). $D = k\lambda/\beta \cos\theta$; D = average crystallite size, K = Scherer coefficient (0.89), $\underline{\lambda}$ = X-ray wavelength ($\underline{\lambda}$–1.5406 Å), θ = Bragg's angle (θ) and β- full width at maximum (FWHM) in radians (Kaviya et al. 2012).

Energy dispersive X-ray spectroscopy

An X-ray microanalyzer (Oxford 6587 INCA, Oxford Instruments, Abingdon, UK) was linked to a transmission electron microscope (TEM) detector (Phillips/FEI CM 120 BioTwin) to determine the elemental composition of the synthesized CCESN. The measurement was conducted after placing the dried sample on a copper grid coated with carbon (Tszyde et al. 2021; Jia et al. 2023).

Energy-dispersive X-ray fluorescence

The Thermo Scientific X-ray Fluorescence (XRF) Epsilon Spectrometer, specifically the energy dispersive X-ray fluorescence (EDXRF) technique, was employed for the elemental identification of the synthesized CCESN. Following a 10-min evacuation with a vacuum pump to eliminate oxygen and moisture from the sample holders, the samples were prepared for analysis using the XRF Spectrometer.

Thermogravimetric analysis

Thermogravimetric Analysis (TGA) of the CCESN was conducted using a TGA 4000 thermal analyzer (Perkin Elmer Life Netherlands) instrument. The analysis involved heating at a rate of 10 °C/min, ranging from 27 to 800 °C, under a nitrogen atmosphere to study the thermal behavior of the synthesized CCESN.

Antibacterial assay
Zone of inhibition

The disk diffusion method was employed to assess the antimicrobial efficacy of the synthesized CCESN against clinical strains of *Staphylococcus saprophyticus* DSM 18669 and *Escherichia coli* 0157 (Hegstad et al. 2014). These strains were sourced from the microbial bank located at the Department of Pharmaceutical Technology, Faculty of Pharmacy, University of Lagos, Idi Araba, Nigeria. Antimicrobial discs containing the synthesized CCESN (40 mg/mL) were placed on Potato Dextrose Agar (PDA) plates using sterile forceps. The placement of the discs on the plates ensured a minimum center-to-center distance of 24 mm, and they were positioned at a distance of at least 10 to 15 mm from the edge of the Petri dish. Standard solutions of pure Levofloxacin were used as a positive control. 0.05 g of Levofloxacin dissolved in 10 mL of sterile distilled water was used to obtain a stock concentration of 5000 mg/mL. Subsequently, a two-fold dilution was performed yielding different concentrations of 0.05, 0.025, 0.0125, and 0.0063 mg/mL (Zulkipli et al. 2022). The zones of inhibition of bacteria were measured in triplicates following a 24-h incubation of the plates at 37 °C (Cyriac et al. 2013).

Minimum inhibitory concentration (MIC)

The broth microdilution assay was used to determine the minimum inhibitory concentration (MIC) (Limam et al. 2011). The synthesized CCESN was diluted in a Giolitti and Cantoni Broth (GCB) medium with a pH of 6 and placed in standard Bioscreen C 100 well microtitre plates. Calibration of the bacterial cell suspension (2×10^8 cfu/mL) was achieved using McFarland 0.5 turbidity standard. After inoculating the test strains into microtitre plates containing 10 mL of prepared normal saline, the plates were then incubated at 37 °C for 24 h. The concentration of the test microorganisms was 1.5×10^8 cfu/mL. After the incubation period, the suspension was

Atanda *et al. J Mater. Sci: Mater Eng.*   (2024) 19:22

Page 5 of 17

additionally diluted in normal saline to achieve a final inoculum with a microbial concentration of 10^8 cfu/mL. The Ag nanocomposite was diluted by a factor of two in sterile broth, commencing at an initial concentration of 40 mg/mL. Subsequent dilutions were prepared at concentrations of 20, 10, 5, 2.5, 1.25, 0.625, 0.3125, 0.1563, 0.0781, 0.0391, 0.0195, and 0.0978 mg/mL, respectively (Nafis et al. 2021). The lowest concentration at which bacterial growth is inhibited is the MIC.

Statistical analysis

The evaluation of antimicrobial test data included calculating means and mean deviations from triplicate determinations. To assess significance, an ANOVA test was performed using GraphPad Software Inc. in San Diego, USA.

Results and discussion

UV–visible spectroscopy

Figure 1a illustrates the transformation of silver ions (Ag^+) into zerovalent silver (Ag^0), manifested by a color shift from off-white to dark brown throughout the reaction. The color change in this study deviated from the color change reported by other authors; a quick transformation from pale brown to yellow–brown color (Perera et al. 2013; Zain et al. 2014). However, the main indicator of a successful noble metal nanoparticle synthesis is a shift in the solution's color (Rezazadeh et al. 2020). According to Sastry et al. (2003), silver nanoparticles were observed to exhibit a diverse range of colors, ranging from light yellow to brown.

A strong peak at λmax$=435$ nm indicates surface plasmon resonance (SPR) that occurs due to the excitation of free ions on the surface of the metal ion signifying the formation of silver nanoparticles (Fig. 1b) (Shukla and Iravani 2018). Additionally, the occurrence of a peak between 200 and 300 nm involving $n \rightarrow \pi^*$ and $\pi \rightarrow \pi^*$ transitions is due to the chelation between chitosan and EDTA (Yan et al. 2014; Kumar et al. 2017). This can also be attributed to charge transfer transitions in the synthesized CCESN. These transitions typically involve the transfer of an electron from a donor (chitosan/EDTA a ligand) to an acceptor (silver atom as metal center) (Kumar 2009; Shweta et al. 2019). Finally, the absence of other peaks within the range of 460 to 1000 nm suggests minimal aggregation of the nanoparticles, which contributes to their overall stability (Gahlawat and Choudhury 2019; Rezazadeh et al. 2020). In the literature, an absorbance peak above 400 nm in the UV–Vis spectrum is widely accepted as an indicator for the formation of AgNPs (Varadavenkatesan, et al. 2020).

Furthermore, the absence of other peaks within the range of 460 to 1000 nm indicates little agglomeration, therefore enhancing the stability of the silver NPs (Gahlawat and Choudhury 2019; Rezazadeh et al. 2020). In the literature, an absorbance peak above 400 nm in the UV–Vis spectrum is widely used as an indicator for the formation of silver NPs (Varadavenkatesan, et al. 2020).

TEM analysis

Figure 2 shows the synthesized CCESN size and shape with 200 nm scale bars. The average size determined with ImageJ software, was 45.30 nm. According to TEM micrographs, the majority of the silver particles exhibited a spherical shape and were polydispersed (Kaviya et al. 2011; Zain et al. 2014; Satapathy et al. 2015; Baran et al. 2023).

The micrographs also showed that a thin layer of chitosan-crosslinked EDTA covered the silver nanoparticles (indicated by a blue arrow in the diagram) thus confirming the capping effect of the crosslinker (Jalilian et al. 2020).

SEM analysis

Figure 3a, b shows the surface morphology and shape of the synthesized CCESN taken at a magnification of 500 and a scale of 100 μm and 300 and a scale of 200 μm respectively consisting of irregularly shaped particles with a rough surface texture. The average size determined with ImageJ software, was 59.45 nm. Figure 3a, b shows darker, well-defined spots and clusters throughout the image are the silver nanoparticles. These nanoparticles are distributed within the chitosan matrix. They appear darker because silver has a higher atomic number and thus scatters electrons more strongly than the surrounding chitosan. The silver nanoparticles vary in size and shape but generally appear as small, roughly spherical, or slightly elongated particles. This is similar to a report by Gupta et al. (2020) on the spherical morphology of chitosan-EDTA silver nanoparticles using a green synthesis approach. However, due to interactions between chitosan and silver nanoparticles, some degree of agglomeration was observed in the SEM images (Koushkaki et al. 2019). Overall, the image demonstrates a successful embedding of silver nanoparticles within a chitosan matrix, potentially modified with EDTA to enhance the binding and stabilization of the nanoparticles. The uniform distribution and the presence of discrete nanoparticles within the matrix are indicative of the successful synthesis of silver nanoparticles.
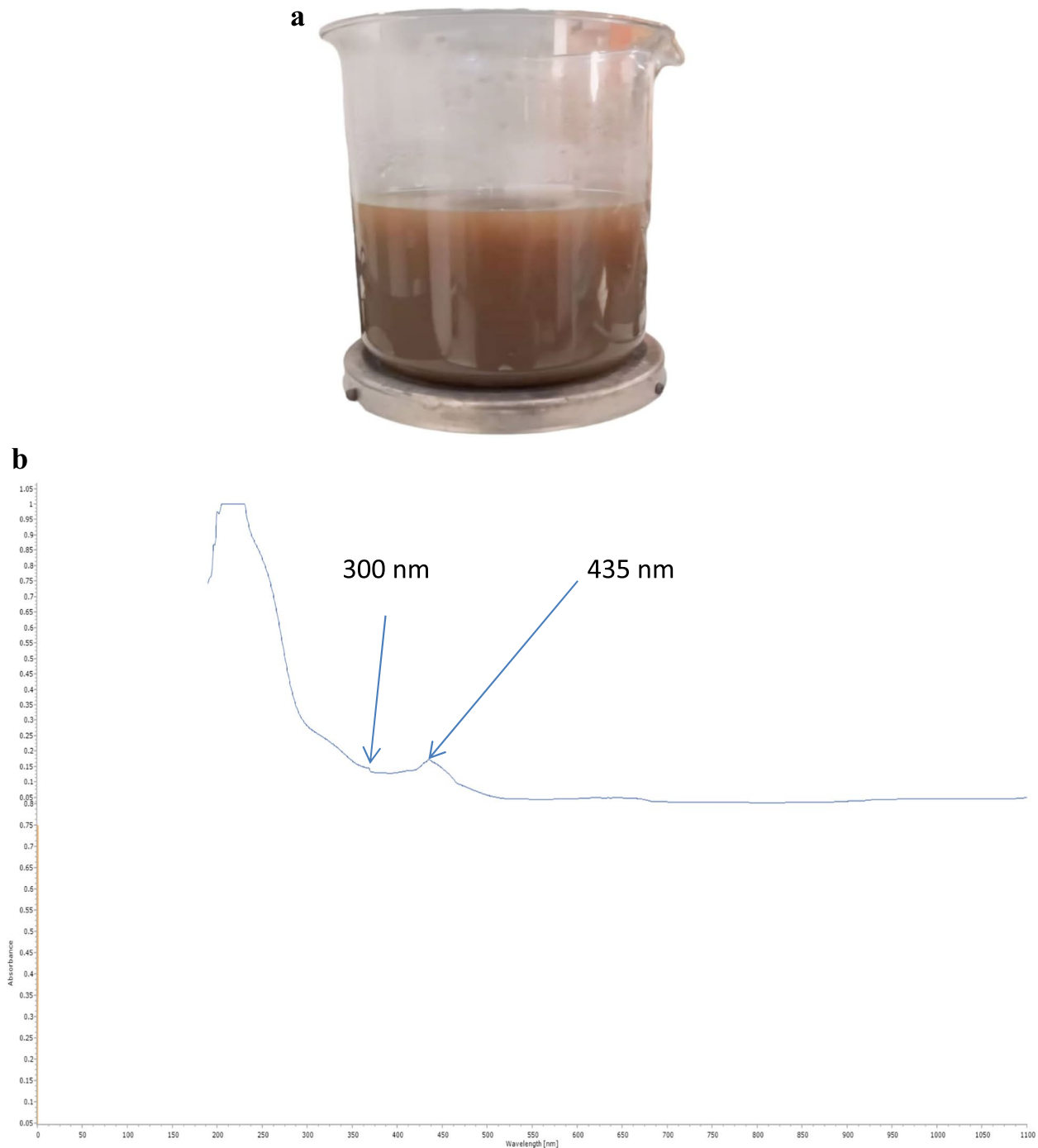
a

b

300 nm   435 nm

Fig. 1 a The CCESN solution after completion of the synthesis. **b** UV–Vis spectrum of the synthesized CCESN

X-ray diffraction pattern

Figure 4 depicts distinct diffraction peaks of the synthesized CCESN. These peaks occur at 38.62°, 42.95°, 45.99°, 52.5°, and 60.01°, indicating the presence of crystalline silver particles. The Miller indices (h k l) for the (111), (200), (220), and (311) planes indicate that the metallic silver atoms have a face-centered cubic (fcc) crystal structure (Helmlinger et al. 2016; Parvathiraja et al. 2021).

The crystallites in the synthesized CCESN have an average size of 22.20 nm, calculated by the Debye–Scherrer equation. These XRD findings align with the TEM results, providing further evidence for the formation of

Atanda *et al. J Mater. Sci: Mater Eng.*   (2024) 19:22

Page 7 of 17
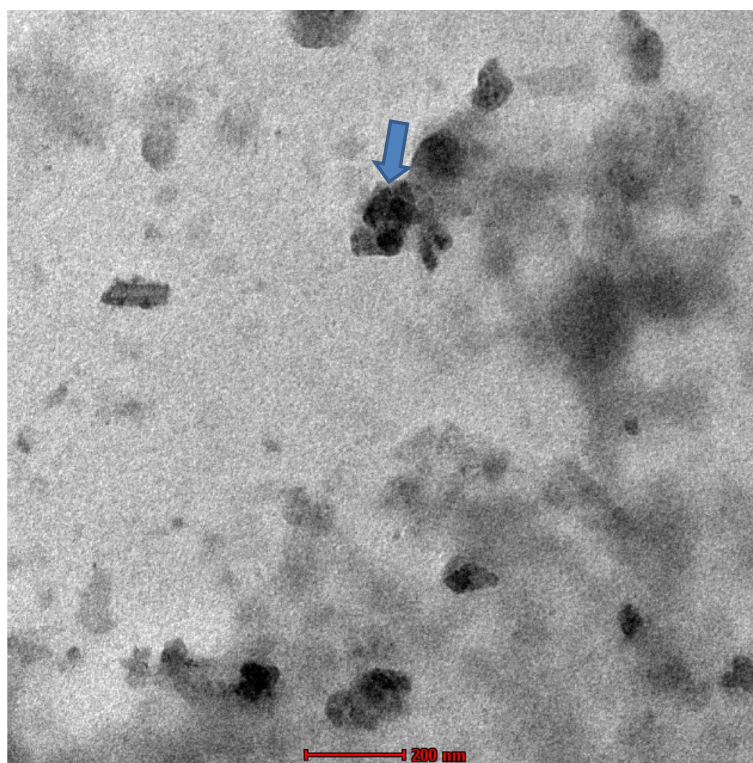
Fig. 2 Micrograph of the synthesized CCESN (200 nm)

silver NPs. It is important to note the presence of comparatively weaker peaks in the X-ray diffraction pattern. These weaker peaks might be attributed to the presence of chitosan and EDTA components within the nanocomposite which are linked to several factors including the semi-crystalline nature of chitosan and EDTA: compared to crystalline silver, chitosan and EDTA are mostly amorphous, meaning they lack a well-defined long-range order in their atomic structure. This characteristic of amorphous materials generally results in weaker and broader peaks in the XRD pattern (Suryanarayana 1998). Lower concentration of chitosan and EDTA: typically, chitosan and EDTA are present in smaller quantities compared to silver in the nanocomposite. According to the principles of X-ray diffraction, the concentration of a crystalline phase can influence the intensity of its corresponding peaks in the pattern (Singh 2011). Therefore, the weaker peaks might be due to the lower concentration of chitosan and EDTA's crystalline phases within the nanocomposite.

EDX profile
Figure 5 shows the EDX spectrum displaying peaks corresponding to several elements, including silver (Ag), carbon (C), oxygen (O), copper (Cu), copper (Cu), and calcium (Ca). The presence of silver peaks within

2.0–3.6 keV confirms the presence of silver nanoparticles in the chitosan-EDTA composite (Vanaja, et al. 2014; Singh et al. 2015; Atalar, et al. 2022). This result also supports the UV Vis (SPR) and XRD results. Carbon and oxygen are likely from the chitosan component (Huang et al. 2016) while copper, iron, sulfur, and calcium may be residual elements from the synthesis process or contaminants (Bjerrum et al. 1958; Rastl et al. 2017). Overall, the EDX profile confirms the presence of silver nanoparticles within the chitosan-EDTA composite, along with other elements likely from chitosan, EDTA, and potentially the synthesis process.

Energy-dispersive X-ray fluorescence
Silver was detected as shown in Fig. 6. At 3.00 keV, a very strong signal was observed; the binding energy typical of silver indicated the formation of silver nanoparticles (Govindan et al. 2012; Satapathy et al. 2015; Parvathiraja et al. 2021). The presence of calcium, silicon, zinc, and iron is due to the chitosan and EDTA. The lack of K and L lines prevented the detection of additional chitosan components such as carbon, and oxygen. The elemental composition from XRD and the EDX spectra, which showed the presence of calcium and other elements, corroborated this finding.
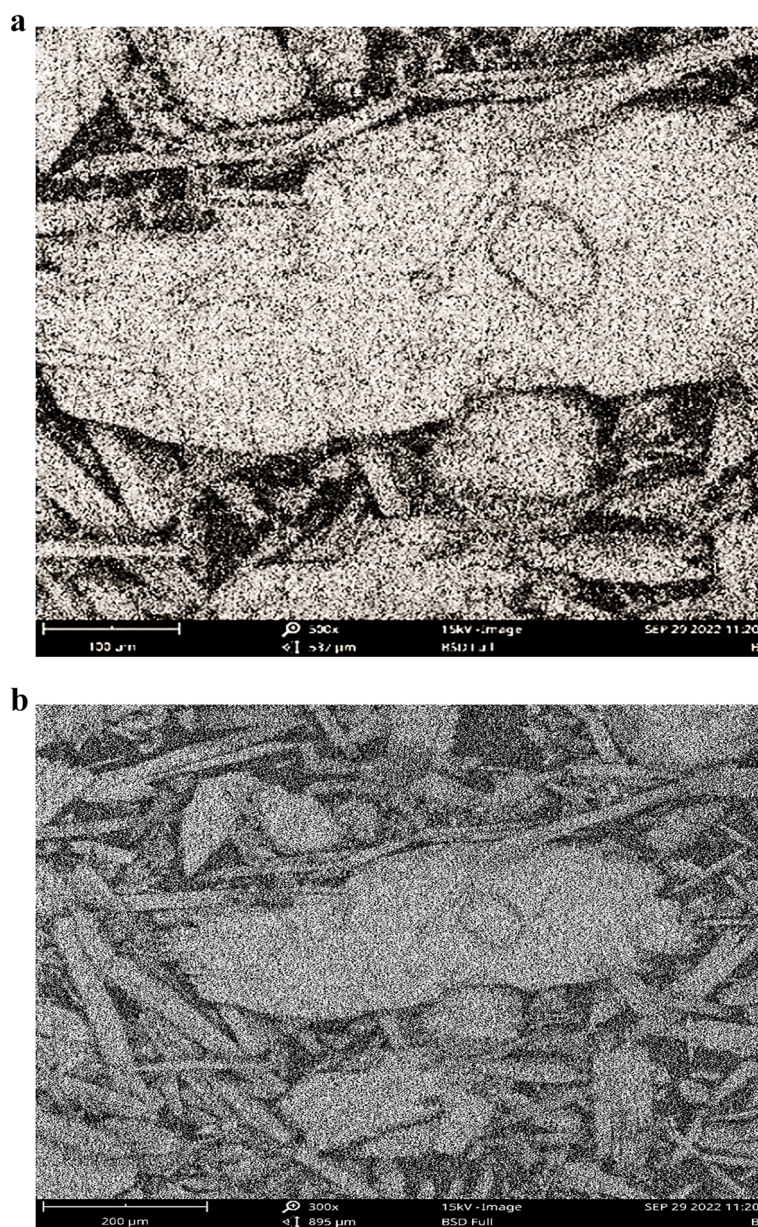
Atanda *et al. J Mater. Sci: Mater Eng.*   (2024) 19:22

Page 8 of 17

Fig. 3 a SEM micrograph of CCESN at a magnification of 300 and 100 μm. **b** SEM micrograph of CCESN at a magnification of 300 and 200 μm

Thermogravimetric analysis

The thermal stability of chitosan and the synthesized CCESN was evaluated under an air atmosphere at the range of 20–800 °C and a rate of 5 °C/min (Fig. 7a, b). Figure 7a shows the TGA profile of chitosan**.** At the first degradation step (a), approximately 89% of the weight is lost around 275 °C. This significant loss is attributed primarily to the removal of physically adsorbed water, impurities, and volatile matter. The high percentage of weight loss in this stage indicates the presence of substantial moisture content and non-bound volatiles within the chitosan. This observation is consistent with findings from similar studies, where initial weight losses are linked to the desorption of water and volatile substances (Kumar et al. 2018).

The second degradation step (b) occurs at around 363 °C, where an additional 57% of weight is lost. This stage corresponds to the removal of amino groups and the onset of degradation of the glycosidic polymer backbone. The breakdown of these components signifies the beginning of the thermal decomposition of chitosan's polymer structure, which is essential for understanding

Atanda *et al. J Mater. Sci: Mater Eng.*   (2024) 19:22

Page 9 of 17
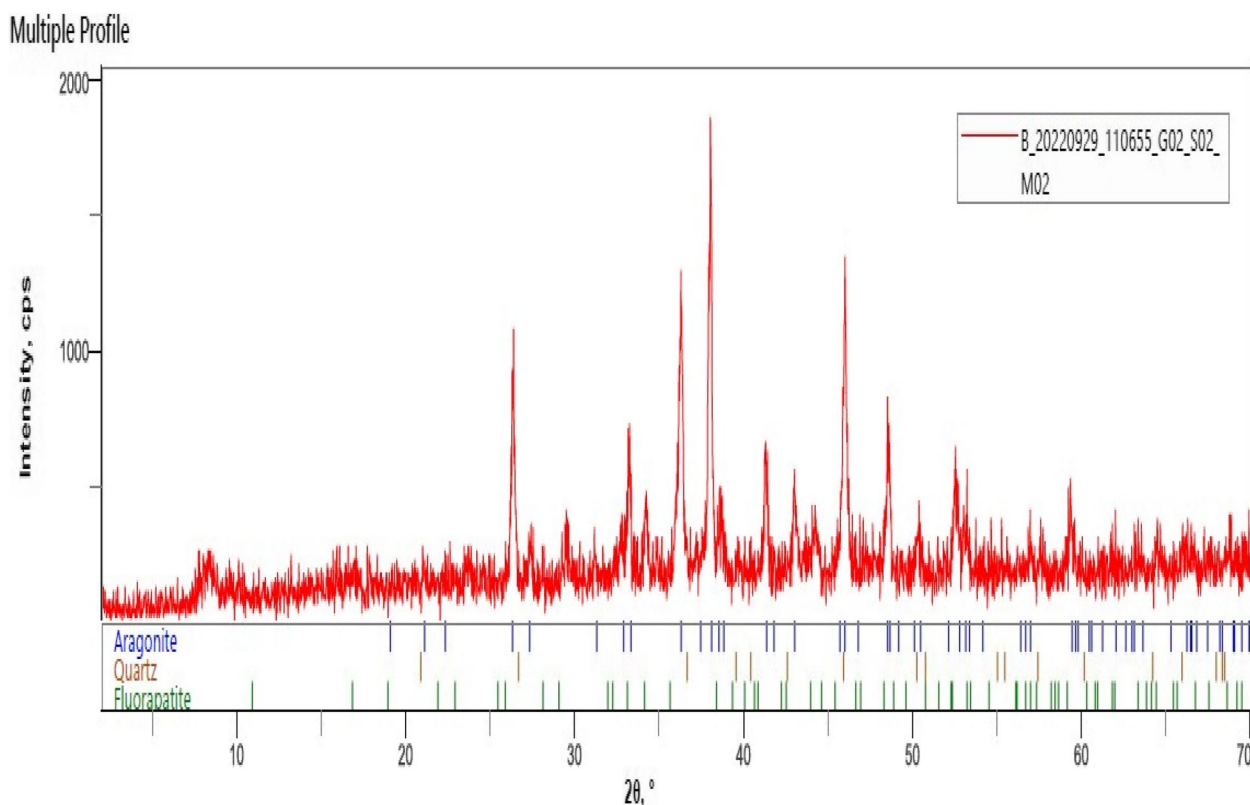
Fig. 4 XRD pattern of synthesized CCESN

its thermal stability and structural integrity. Recent literature supports this observation, highlighting the critical role of amino groups and glycosidic bonds in the thermal decomposition process (Alves et al. 2019).

During the third degradation step (c), occurring at approximately 438 °C, chitosan experiences an additional weight loss of about 18%. This weight loss is associated with the further degradation of the glycosidic polymer backbone and other side chains. The continued breakdown of the polymer chain reflects the progressive decomposition of chitosan's structural elements, resulting in a more complex mixture of degradation products. This behavior aligns with findings from recent studies, which document the ongoing decomposition of chitosan's polymeric structure (Zhang et al. 2020a, b).

In the fourth degradation step (d), at around 610 °C, chitosan has lost about 9% of its weight. This final stage of weight loss is associated with the formation of amorphous carbon materials, charred aromatic residues, and oxides of metals present in chitosan. The residual weight loss indicates the formation of a carbonaceous char and potentially inorganic residues, reflecting chitosan's ability to form stable carbon residues at high temperatures. This result provides insights into the material's behavior under extreme conditions and aligns with observations

from recent research on the thermal stability of chitosan (Melo et al. 2021).

Figure 7b shows the TGA profile of CCESN. The first degradation (a) occurred around 156 °C with a weight loss of 97%. This weight loss corresponds to the removal of moisture, physically adsorbed water, or volatile components in the nanocomposite. The second degradation (b) occurred around 311 °C with a weight loss of 96%. This weight loss in this region can be attributed to the depolymerization and decomposition of chitosan polymer chains and EDTA molecules (desorption process). Also, this can be attributed to the stabilization/capping and reduction of silver NP. The addition of EDTA may influence the onset temperature and extent of degradation in this step, indicating potential interactions or modifications to the nanocomposite structure. The third degradation (c) and fourth degradation (d) occurred around 363 °C and 464 °C with a weight loss of 18% of 68% respectively. The weight loss in these regions is an indication of the decomposition or oxidation of silver nanoparticles. Changes in temperature and weight loss patterns in this step can indicate specific interactions between the chitosan, EDTA, and silver, as a result of complexation, coordination, or phase changes. Also, silver ions might interact with chitosan, affecting its
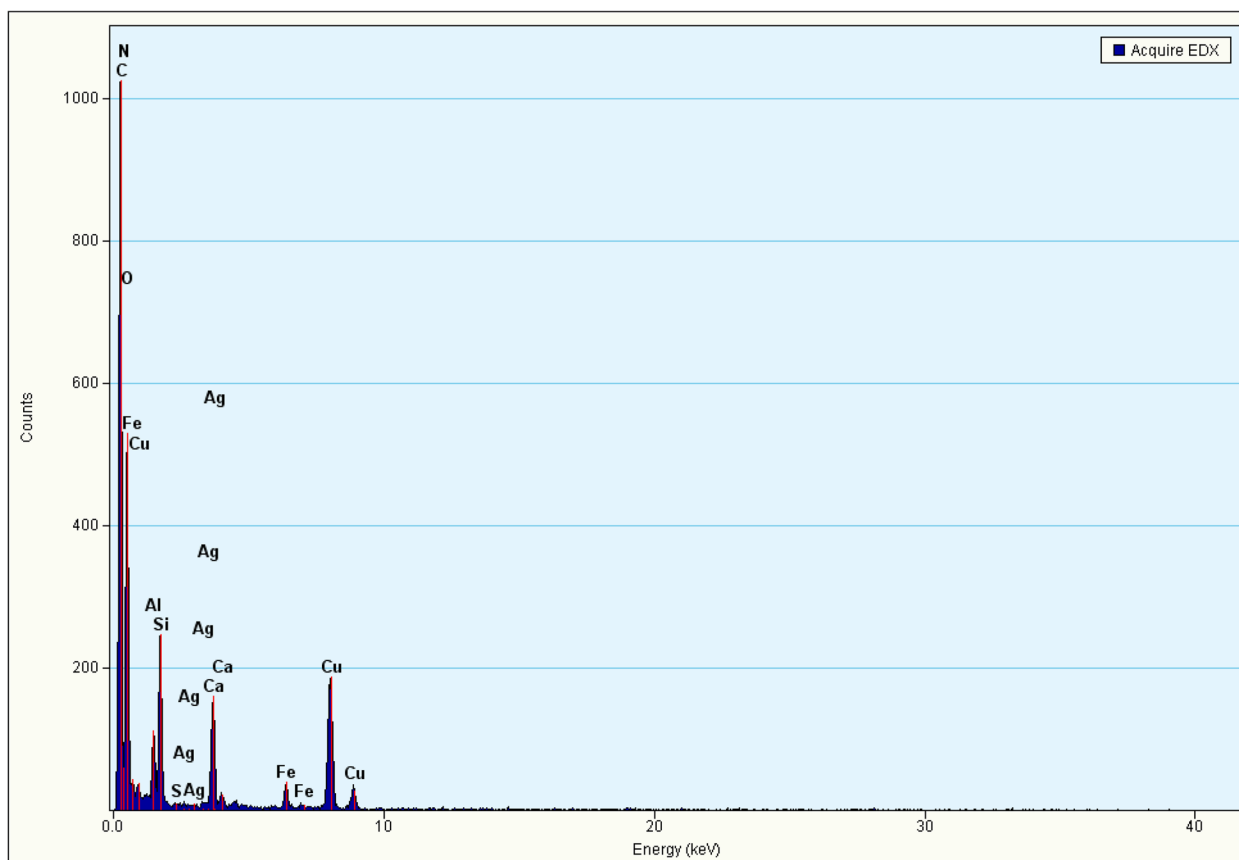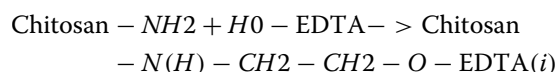
Fig. 5 EDX spectrum of the synthesized CCESN

thermal stability and leading to additional decomposition steps. Furthermore, the highest temperature at this stage is an attestation to the existence of Ag nanoparticles hence thermal stability of the nanocomposite was altered (Parvez et al. 2012; Maciel et al. 2015). The multiple degradation steps likely reflect complex interactions between chitosan, EDTA, and silver components. The presence of additives or metals can influence the final stages of degradation, potentially altering the formation of residues or ash and affecting the overall thermal stability of the material. Overall, this phenomenon is vital for designing and implementing heterogeneous biomedical and medical sensing and imaging applications, which need to be recycled and heated repeatedly during thermal reactivation.

Step-by-step chemical reactions for CCSEN formation

The formation of the CCSEN can be represented by a series of chemical reactions:
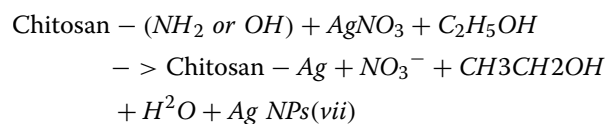
1. *Potential crosslinking between chitosan and EDTA*

$$Chitosan - NH2 + H0 - EDTA- > Chitosan - N(H) - CH2 - CH2 - O - EDTA (i)$$

2. *Interaction between chitosan and silver ions*

$$Chitosan - NHg2 + AgNO_3 \rightarrow Chitosan - NH_2^+ + NO_3^- + Ag^+ (ii)$$
$$Chitosan - OH + AgNO_3- > Chitosan - O^- + NO_3^- + Ag^+ (iii)$$
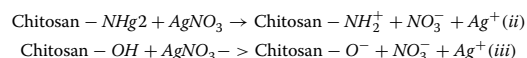
3. *Reduction of silver ions by ethanol*

$$C_2H_5OH + H^+ - > CH_3CH_2O^+ + H_2 (iv)$$
$$CH_3CH_2O^+ + e^- - > CH_3CH_2OH (v)$$
$$2Ag^+ + 2e^- - > 2Ag (vi)$$
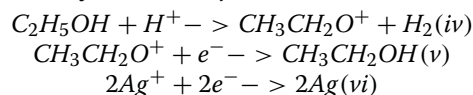
Overall formation reaction

$$Chitosan - (NH_2 \text{ or } OH) + AgNO_3 + C_2H_5OH$$
$$- > Chitosan - Ag + NO_3^- + CH3CH2OH$$
$$+ H^2O + Ag \ NPs (vii)$$

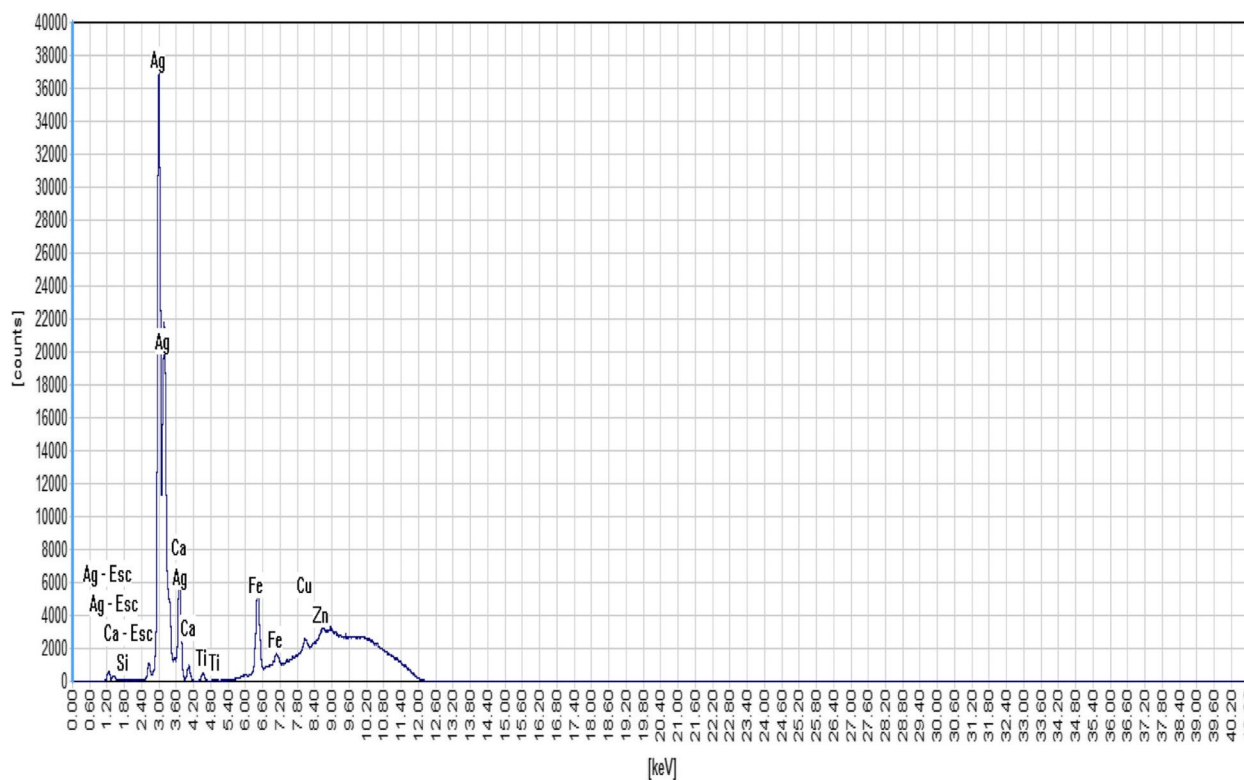Atanda *et al. J Mater. Sci: Mater Eng.*   (2024) 19:22

Page 11 of 17

Fig. 6 EDXRF spectrum of the synthesized CCESN

Mechanism of formation synthesized CCESN: interaction between chitosan, EDTA, and silver nanoparticles

We proposed that the synthesized CCESN occurred via an additional reaction (NH_2 group from chitosan and OH from EDTA) leading to a polymeric chain. The polar hydroxyl and ether groups of chitosan are expected to interact with electropositive silver cations. As a result, $AgNO_3$ combined with chitosan solution in the presence of ethanol; Ag^+ ions may form electrostatic (ion–dipole) interactions with chitosan macromolecules. Furthermore, ethanol, acting as a protic solvent, supplies electrons to reduce silver ions into zerovalent silver (Chou et al. 2005). Ag nanoparticles were synthesized through the reduction of Ag^+ utilizing ethanol and chitosan as the reducing and stabilizing agents, respectively. Chitosan contains hydroxyl groups that aid in the passivation of the particle surfaces. In the absence of this passivation, the nanoparticles would aggregate due to their elevated surface energies. The proposed structure of the synthesized CCESN is depicted in Fig. 8. The interaction between chitosan and silver nanoparticles in the composite is a crucial aspect of its antimicrobial activity. Chitosan due to the presence of hydroxyl and amino groups stabilizes silver nanoparticles, limiting their aggregation and enhancing

their bioavailability (Zhang et al. 2020a, b). Additionally, chitosan possibly reduces the toxicity of silver nanoparticles by binding to their surface and preventing their interaction with cellular components (Saha et al. 2020). The interaction between chitosan and silver nanoparticles also enhances the antimicrobial activity of the composite, as chitosan helps silver nanoparticles penetrate deeper into microbial cells (Tran et al. 2019).

Antibacterial study

The analysis of the antimicrobial activity of the synthesized CCESN and Levofloxacin against *S. saprophyticus* DSM 18669 and *E. coli* strain 0157 (Figs. 9a, b and 10a, b) reveals significant insights with substantial practical implications. The synthesized CCESN demonstrated a remarkably larger zone of inhibition (46.0 mm) against *S. saprophyticus* compared to all tested concentrations of Levofloxacin (Table 1). This indicates its superior antibacterial efficacy. Statistical analysis confirms that the inhibition zones for the silver nanocomposite are significantly larger than those for levofloxacin, underscoring its potent antimicrobial properties.

In contrast, for *E. coli*, the silver nanocomposite at the same concentration showed a zone of inhibition of 25.70 mm (Table 2). Levofloxacin at 0.05 mg/
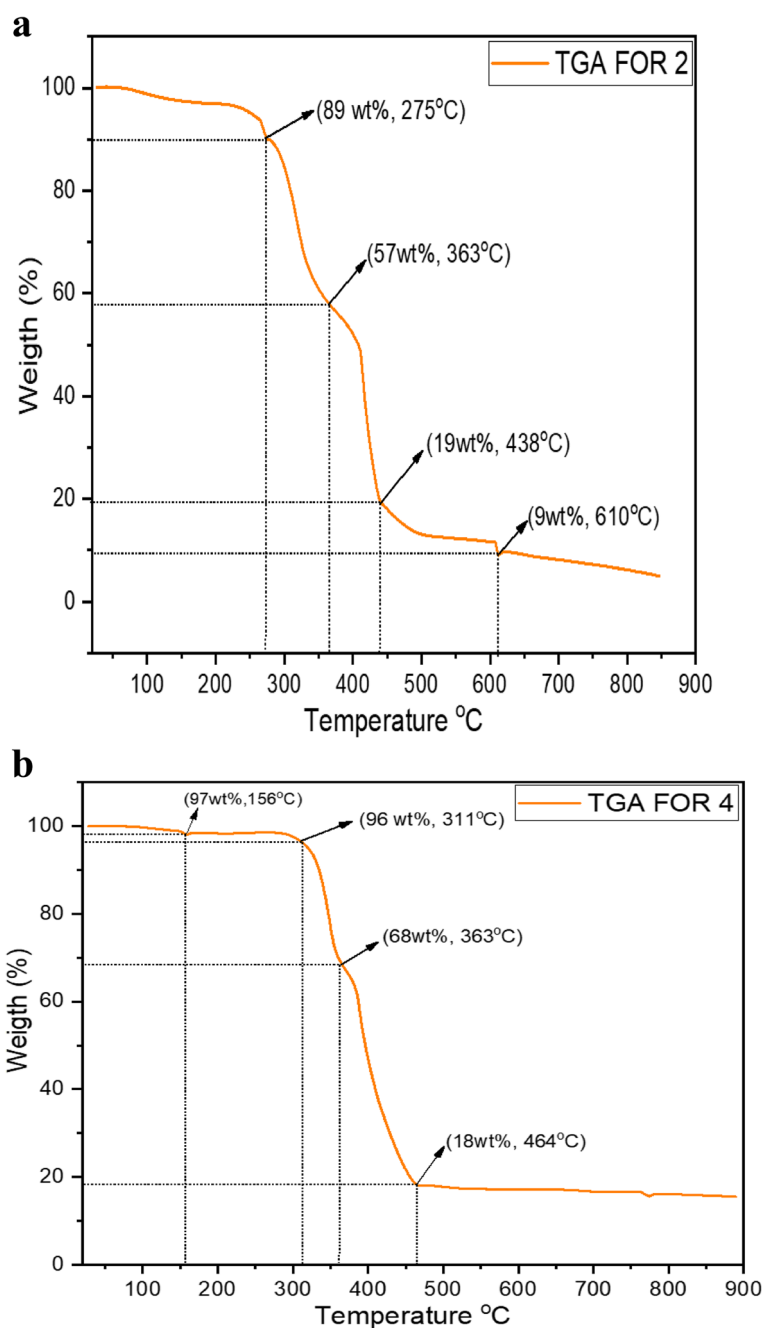
Fig. 7 a Thermogram profile of the synthesized chitosan; a (initial degradation); b (second degradation); **c** (third degradation); d (fourth degradation). **b** Thermogram profile of the synthesized CCESN; a (initial degradation); b (second degradation); c (third degradation); d (fourth degradation)

mL exhibited a larger zone of inhibition (30.33 mm), indicating higher effectiveness at this concentration. However, the silver nanocomposite demonstrated comparable effectiveness to levofloxacin at lower concentrations (0.025 mg/mL and 0.0125 mg/mL). Notably, no inhibition was observed for levofloxacin at 0.0063 mg/mL, whereas the silver nanocomposite maintained antibacterial activity, indicating its potential for sustained effectiveness at lower concentrations.

The findings underscore the potential of silver nanoparticles synthesized with chitosan-EDTA as potent antimicrobial agents, particularly against *S. saprophyticus.* This effectiveness makes them suitable for various applications, including medical devices, coatings, and
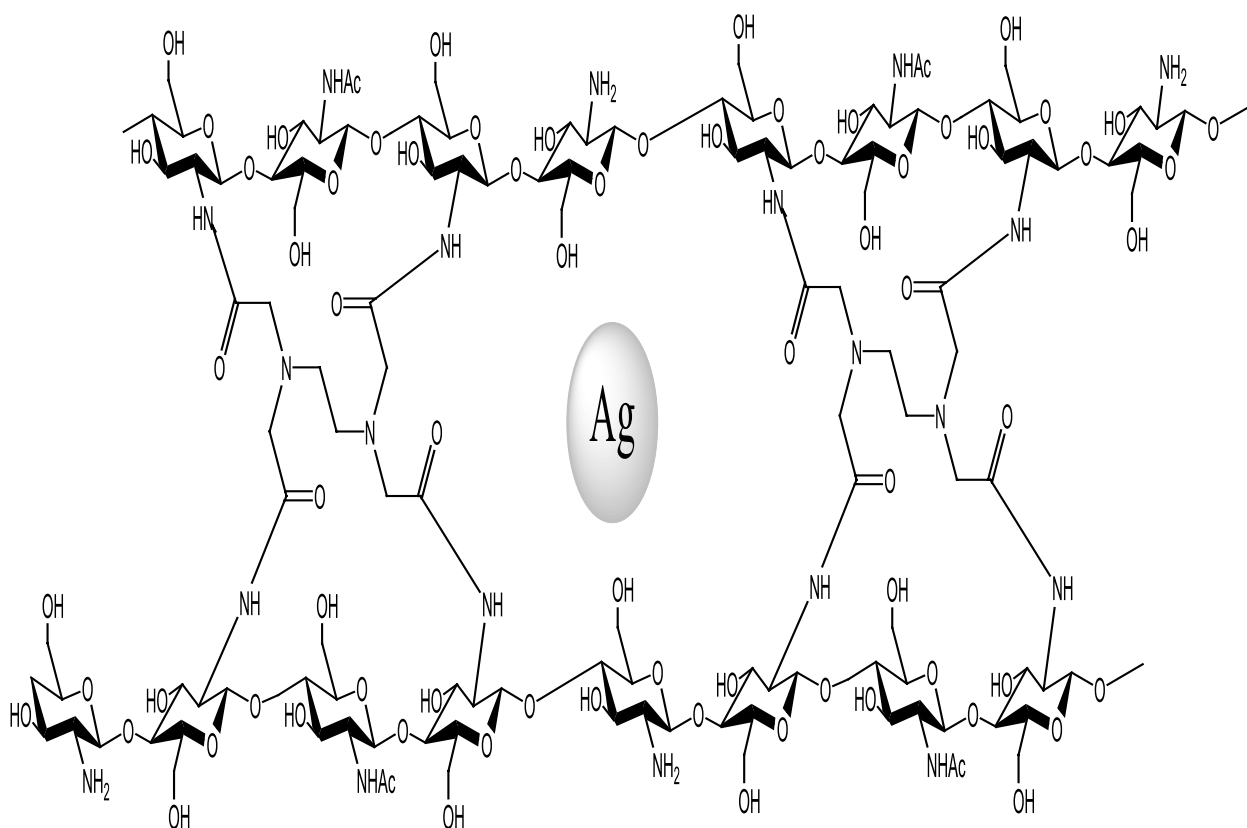
Fig. 8 Proposed structure of the synthesized CCESN

a	b
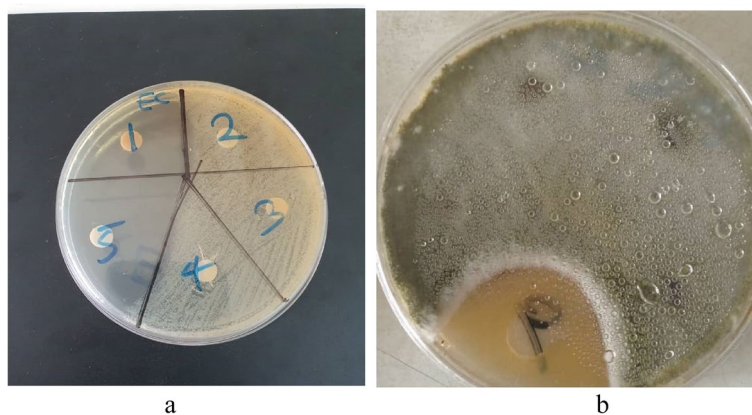
Fig. 9 Zone of inhibition of synthesized CCESN against **a** *Staphylococcus saprophyticus* DSM 18669. **b** *Escherichia coli* strain 0157

treatments aimed at preventing bacterial contamination. The differential effectiveness against *S. saprophyticus* and *E. coli* emphasizes the importance of selecting antimicrobial treatments based on the specific bacterial strain being targeted.

The minimum inhibitory concentration (MIC) values for the synthesized CCESN against both strains are identical, as shown in Table 3 (0.0781 mg/mL). This suggests that the synthesized CCESN may have a bactericidal effect, completely inhibiting bacterial growth, rather than a bacteriostatic effect, which only halts growth (Zain et al. 2014).

The observed difference in susceptibility between the two bacterial strains can be attributed to the variations

Atanda *et al. J Mater. Sci: Mater Eng.*   (2024) 19:22

Page 14 of 17
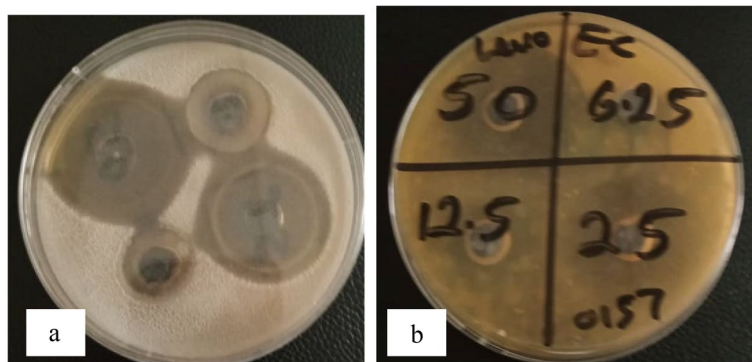
Fig. 10 Zone of inhibition of levofloxacin **a** *Staphylococcus saprophyticus* DSM 18669 and **b** *Escherichia coli* strain 0157

Table 1 Inhibition zone for *Staphylococcus saprophyticus* DSM 18669

Sample	Concentration (mg/mL)	Zone of inhibition (mm)
Silver nanocomposite	40	$46.0^a \pm 0.82$
Levofloxacin	0.05	$31.33^c \pm 0.4$
	0.025	$27.33^c \pm 0.24$
	0.0125	$24.50^c \pm 0.41$
	0.0063	$18.33^b \pm 0.23$

a, *b*, and *c* are statistically significant while *b* is statistically insignificant ($p < 0.05$)

Table 2 Inhibition zone for *Escherichia coli strain 0157*

Sample	Concentration (mg/mL)	Zone of inhibition (mm)
Silver nanocomposite	40	$25.70^a \pm 0.25$
Levofloxacin	0.05	$30.33^b \pm 0.24$
	0.025	$25.50^b \pm 0.41$
	0.0125	$20.17^b \pm 0.24$
	0.0063	0.00

a and *b* are statistically significant while *b* is statistically insignificant ($p < 0.05$)

Table 3 Minimum inhibitory concentration of Ag nanocomposite against the bacterial strains

Strains	MIC (mg/ mL)
Staphylococcus saprophyticus DSM 18669	0.0781
Escherichia coli strain 0157	0.0781

in their cell wall structure (Pasquina-Lemonche et al. 2020). Gram-positive bacteria possess a thicker cell wall composed of a more substantial peptidoglycan layer compared to the thinner layer found in Gram-negative bacteria (Shukla et al. 2013). Additionally, the surface of bacteria carries a negative charge due to the presence of carboxylic acids and other groups (Stoimenov et al. 2002).

The likely mechanism of action for the CCESN against *S. saprophyticus* DSM 18669 involves the release of silver cations from the nanoparticles. These cations are attracted to the negatively charged bacterial surface and bind to it. This binding disrupts the bacterial membrane integrity, ultimately leading to cell death (Li et al. 2008; Kaviya et al. 2011).

It's important to note that there is no definitive consensus on whether Gram-positive bacteria are inherently more resistant to antimicrobials compared to Gram-negative bacteria (Ahmed et al. 2022).

Conclusion

This study provides an alternative pathway to the synthesis of silver NPs from the chitosan-modified EDTA. The chitosan was derived from the shells of *A. marginata* considered agricultural wastes. This method is sustainable, cost-effective, and environmentally friendly. The confirmation of silver formation in the nanocomposite was achieved through various characterization techniques, including TEM, SEM, XRD, EDX, EDXRF, TGA, and UV–visible. The antibacterial activity of the CCESN is comparable to Levofloxacin, while it exhibited the same identical Minimum Inhibitory Concentration (MIC) values against both strains. Consequently, the synthesized CCESN holds promise for diverse antibacterial applications such as medical implants, bioactive food packaging systems, and drug delivery.

Atanda *et al. J Mater. Sci: Mater Eng.*   (2024) 19:22

Page 15 of 17

Declarations

References
Ahmed HY, Safwat N, Shehata R, Althubaiti EH, Kareem S, Atef A, Qari SH, Aljahani AH, Al-Meshal AS, Youssef M, Rokayya SR (2022) Synthesis of natural nano-hydroxyapatite from snail shells and its biological activity: antimicrobial, antibiofilm, and biocompatibility. Membranes 12:408. https://doi.org/10.3390/membranes12040408

Ali I, Gupta VK (2006) Advances in water treatment by adsorption technology. Nat Protoc 1(6):2661–2667

Almalah H, Alzahrani HA, Abdelkader HS (2019) Green synthesis of silver nanoparticles using *Cinnamomum zylinicum* and their synergistic effect against multi-drug resistance bacteria. J Nanotechnol Res 1:95–107

Almalik A, Benabdelkamel H, Masood A, Alanazi IO, Alradwan I, Majrashi MA, Alfadda AA, Alghamdi WM, Alrabiah H, Tirelli N, Alhasan AH (2017) Hyaluronic acid coated chitosan nanoparticles reduced the immunogenicity of the formed protein corona. Sci Rep 7:10542. https://doi.org/10.1038/s41598-017-10836-7

Alves H, de Oliveira D, Silva R (2019) Thermal degradation and kinetic study of chitosan-based materials. Carbohyd Polym 207:362–370

Atalar MN, Baran A, Baran MF, Keskin C, Aktepe N, Yavuz Ö, İrtegunKandemir, S. (2022) Economic fast synthesis of olive leaf extract and silver nanoparticles and biomedical applications. Part Sci Technol. 40:589–597

Baran A, Keskin C, Baran MF, Huseynova I, Khalilov R, Eftekhari A, Irtegun-Kandemir S, Kavak DE (2021) Ecofriendly synthesis of silver nanoparticles using *Ananas comosus* fruit peels: anticancer and antimicrobial activities. Bioinorg Chem Appl 2021:2058149

Baran MF, Keskin C, Baran A, Hatipoğlu A, Yildiztekin M, Küçükaydin S, Kurt K, Hoşgören H, Sarker MMR, Sufianov A (2023) Green synthesis of silver nanoparticles from *Allium cepa* L. peel extract, their antioxidant, antipathogenic, and anticholinesterase activity. Molecules 28:2310. https://doi.org/10.3390/molecules28052310

Bjerrum J, Schwarzenbach G, Sillén LG (1958) Stability constants of metal-ion complexes with inorganic ligands. The Chemical Society, London

Chen Y, Zhang J, Zheng X (2019) Chitosan-based composites for the removal of heavy metals from aqueous solutions: a review. Sci Total Environ 658:1049–1065

Chou KS, Lu YC, Lee HH (2005) Effect of alkaline ion on the mechanism and kinetics of chemical reduction of silver Science Direct In Kildeby, N. L., Andersen, O.Z., Cyriac, M. B., Vidya, P., Manjula, S. & Maji, J. (2013). Antimicrobial properties of coconut husk aqueous extract on cariogenic bacteria. Arch Med Health Sci 1(2):126–130

Costa IF, Pires GP, Espínola JG, Brito HF, Felinto MC, Faustino WM, Teotonio EE (2020) Luminescence properties of the Ln–EDTA complexes covalently linked to the chitosan biopolymers containing β-diketonate as antenna ligands. Luminescence 35(3):365–372. https://doi.org/10.1002/BIO.3735

Cyriac MB, Vidya P, Manjula S, Maji J (2013) Antimicrobial properties of coconut husk aqueous extract on cariogenic bacteria. Arch Med Health Sci 1(2):126–130. https://doi.org/10.4103/2321-4848.123024

de Marco A, Chua E, Alink L, Kopylov M (2023) Square beams for optimal tiling in TEM. https://doi.org/10.21203/rs.3.rs-3220524/v1

Dhaka A, Mali SC, Sharma S, Trivedi R (2023) A review on biological synthesis of silver nanoparticles and their potential applications. Results Chem 6:101108. https://doi.org/10.1016/j.rechem.2023.101108

Gahlawat G, Choudhury AR (2019) A review on the biosynthesis of metal and metal salt nanoparticles by microbes. RSC Adv 9:12944–12967

Govindan S, Nivethaa EAK, Saravanan R, Narayanan V, Stephen A (2012) Synthesis and characterization of chitosan–silver nanocomposite. Appl Nanosci 2:299–303. https://doi.org/10.1007/s13204-012-0109-5

Gupta D, Prasad R, Pandey AK, Varma A (2020) Green synthesis of chitosan-EDTA supported silver nanoparticles for enhanced antimicrobial activity. Int J Biol Macromol 162:1215–1226 https://www.sciencedirect.com/science/article/abs/pii/S0144861718308300

Hadrup N, Lam HR (2019) Silver nanoparticles: a review of toxicological and antimicrobial properties. Toxicol Vitro 57:297–306

Hajialyani M, Tewari D, Sobarzo-Sánchez E, Nabavi SM, Farzaei MH, Abdollahi M (2018) Natural product-based nanomedicines for wound healing purposes: therapeutic targets and drug delivery systems. Int J Nanomed 13:5023–5043. https://doi.org/10.2147/IJN.S174072. PMID:30214204;PMCID:PMC6128268

Hegstad K, Giske CG, Haldorsen B, Matuschek E, Schønning K, Leegaard TM, Kahlmeter G, Sundsfjord A, NordicAST VRE Detection Study Group (2014) Performance of the EUCAST disk diffusion method, the CLSI agar screen method, and the Vitek 2 automated antimicrobial susceptibility testing system for detection of clinical isolates of Enterococci with low- and medium-level VanB-type vancomycin resistance: a multicenter study. J Clin Microbiol 52(5):1582–9. https://doi.org/10.1128/JCM.03544-13. Epub 2014 Mar 5. PMID: 24599985; PMCID: PMC3993630

Helmlinger J, Prymak O, Loza K, Gocyla M, Heggen M, Epple M (2016) On the crystallography of silver nanoparticles with different shapes. Cryst. Growth Des 16:3677–3687. https://doi.org/10.1021/acs.cgd.6b00178

Huang Y, Ou W, Yang Y (2016) Chitosan-based nanomaterials for antibacterial applications. Polymers 8(8):246 https://www.mdpi.com/2362050

Jalilian F, Chahardoli A, Sadrjavadi K, Fattahi A, Shokoohinia Y (2020) Green synthesized silver nanoparticle from *Allium ampeloprasum* aqueous extract: characterization, antioxidant activities, antibacterial and cytotoxicity effects. Adv Powder Technol 31:1323–1332

Jia MS, Hash S, Reynoso W, Elsaadany M, Ibrahim H (2023) Characterization and biocompatibility assessment of boron nitride magnesium nanocomposites for orthopedic Aapplications. Bioengineering 10(7):757. https://doi.org/10.3390/bioengineering10070757

Kaur R, Singh K, Agarwal S, Masih M, Chauhan A, Gautam PK (2023) Silver nanoparticles induces apoptosis of cancer stem cells in head and neck cancer. Toxicol Rep 12:10–17. https://doi.org/10.1016/j.toxrep.2023.11.008. PMID:38173651;PMCID:PMC10758978

Kaviya S, Santhanalakshmi J, Viswanathan B, Muthumary J, Srinivasan K (2011) Biosynthesis of silver nanoparticles using *Citrus sinensis* peel extract

and its antibacterial activity. Spectrochim Acta A Mol Biomol Spectrosc 79:594–8. https://doi.org/10.1016/j.saa.2011.03.040

Kaviya S, Santhanalakshmi J, Viswanathan B (2012) Biosynthesis of silver nano-flakes by *Crossandra infundibuliformis* leaf extract. Mater Lett 67(1):64–66. https://doi.org/10.1016/j.matlet.2011.09.023

Khan S, Ullah S, Khan T (2019) Comparative study of antimicrobial activity of chitosan and silver nanoparticles against pathogenic microorganisms. J Nanopart Res 21(10):1–12

Khwannimit D, Jaikrajang N, Dokmaisrijan S, Rattanakit P (2019) Biologically green synthesis of silver nanoparticles from *Citrullus lanatus* extract with L-cysteine addition and investigation of colourimetric sensing of nickel(II) potential. Mater Today 17(4):2028–2038. https://doi.org/10.1016/j.matpr.2019.06.251

Koushkaki M, Abbaszadeh M, Aghazadeh A (2019) Synthesis and characteriza-tion of Chitosan-EDTA/Silver nanocomposites for antibacterial applica-tions. J Inorg Organomet Polym Mater 29(6):2082–2091

Krithiga N, Rajalakshmi A, Jayachitra A (2015) Green synthesis of silver nano-particles using leaf extracts of *Clitoria ternatea* and *Solanum nigrum* and study of its antibacterial effect against common nosocomial pathogens. J Nanosci 2015:928204. https://doi.org/10.1155/2015/928204

Krutyakov YA, Kudrinskiy AA, Olenin A, Lisichkin GV (2008) Synthesis and properties of silver nanoparticles: advances and prospects. Russ Chem Rev 77:233–257

Kumar S, Khan MR, Cameotra SS (2017) Chitosan-EDTA conjugate: a potential adsorbent for removal of heavy metals from water. J Environ Chem Eng 5(4):3441–3448

Kumar R, Nair PR, Sharma A (2018) Thermogravimetric analysis of chitosan and its derivatives. J Therm Anal Calorim 134(2):1055–1064

Kumar P, Kumar V, Mahapatra SK (2020) Chitosan-based nanomaterials for antimicrobial applications. J Mater Sci 55(10):4311–4333

Kumar CSSR (2009) Metallic nanomaterials. Nanomaterials for the Life Sciences, Volume 1. Weinheim: Wiley-VCH, p 571 https://doi.org/10.1002/anie.200903699

Kvitek L, Panacek A, Prucek R, Soukupova J, Vanickova M, Kolar M, Zboril R (2019) Nanosilver and the immune system. J Control Release 294:237–246. https://doi.org/10.1016/j.jconrel.2018.12.011

Li S (2024) Quantitative characterization by transmission electron microscopy and its application to interfacial phenomena in crystalline materials. Materials 17(3):578. https://doi.org/10.3390/ma17030578

Li W-R, Xie X-B, Shi Q-S, Duan S-S, Ouyang Y-S, Chen Y-B (2008) Antibacte-rial effect of silver nanoparticles on Staphylococcus aureus. Biometals 21(3):397–404. https://doi.org/10.1007/s10534-008-9128-9

Limam Z, Selmi S, Sadok S, El Abed A (2011) Extraction and characterization of chitin and chitosan from crustacean by-products: biological and physicochemical properties. Afr J Biotechnol 10(4):640–647. https://doi.org/10.5897/AJB10.209

Lin Y, Jing W, Kang P, Xiaoming Z, Zhouping W, Wenshui X (2011) Prepara-tion and characterization of core/shell-type Ag/chitosan nanoparti-cles. Bull Korean Chem Soc 32(4):1277–1282

Liu X, Zhang W, Liu H (2020a) Enhanced removal of heavy metals from aqueous solutions by EDTA-modified chitosan. J Environ Chem Eng 8(5):103945

Liu Y, He L, Mustapha A (2020b) Antimicrobial properties of nanosilver against foodborne pathogens. J Food Sci 85(5):S1448–S1456

Maciel VBV, Yoshida CMP, Franco TT (2015) Development of a nanocomposite film based on pectin and silver nanoparticles with antimicrobial activ-ity and improved thermal and mechanical properties. Food Hydro-coll 48:292–299. https://doi.org/10.1016/j.foodhyd.2015.02.026

Marambio-Jones C, Hoek EMV (2010) A review of the antibacterial effects of silver nanomaterials and potential implications for human health and the environment. J Nanopart Res 12(5):1531–1551

Martin Z, Gomez MA, Jimenez I (2010) Electron microscopy (TEM) and X-ray Spectromicroscopy (STXM) of PP/MMT/PP-g-MA and PP/MMT/SEBS Nanocomposites. MRS Online Proc Libr 1257:809. https://doi.org/10.1557/PROC-1257-O08-09

Melo M, Pereira M, Campos J (2021) Char formation and thermal stability of chitosan-based materials. J Anal Appl Pyrol 155:105083

Mirzazadeh TFS, Hajiramezanali M, Geramifar P, Raouf M, Dinarvand R, Soleimani M, Atyabi F (2020) Controlling evolution of protein corona: a prosperous approach to improve chitosan-based nanoparticle biodistri-bution and half-life. Sci Rep (nature Publisher Group) 10:1–4

Mohammed MA, Syeda JTM, Kishor KM, Wasan EK (2017) An overview of chi-tosan nanoparticles and its application in non-parenteral drug delivery. Pharmaceutics 9:53. https://doi.org/10.3390/pharmaceutics9040053

Nafis A, Iriti M, Ouchari L, El Otmani F, Marraiki N, Elgorban AM, Syed A, Mezrioui N, Hassani L, Custódio L (2021) New insight into the chemi-cal composition, antimicrobial and synergistic effects of the Moroccan endemic *Thymus atlanticus* (Ball) Roussine essential oil in combination with conventional antibiotics. Molecules 26(19):5850. https://doi.org/10.3390/molecules26195850

Oyekunle DT, Omoleye JA (2019) New process for synthesizing chitosan from snail shells. J Phys Conf Ser 1299:012089. https://doi.org/10.1088/1742-6596/1299/1/012089

Parvathiraja C, Shailajha S, Shanavas S, Gurung J (2021) Biosynthesis of silver nanoparticles by Cyperus pangorei and its potential in structural, optical and catalytic dye degradation. Appl Nanosci 11:477–91. https://doi.org/10.1007/s13204-020-01585-7

Parvez S, Kang M, Chung HS, Bae H (2012) Thermal stability and enhanced mechanical properties of silver-reinforced nanocompos-ites. J Appl Polym Sci 124(5):3960–3967. https://doi.org/10.1002/app.35449

Pasquina-Lemonche L, Burns J, Turner RD, Kumar S, Tank R, Mullin N, Wilson JS, Chakrabarti B, Bullough PA, Foster SJ, Hobbs JK (2020) The architecture of the gram-positive bacterial cell wall. Nature 582:294–297

Perera S, Bhushan B, Bandara R, Rajapakse G, Rajapakse S, Bandara C (2013) Morphological, antimicrobial, durability, and physical properties of untreated and treated textiles using silver-nanoparticles. Colloids Surf A 436:975–989

Putri KN, Siswanta D, Suherman S (2019) Synthesis of EDTA-crosslinked chito-sancarboxymethyl cellulose film as Cu(II) adsorbent, p 75–85

Rajeshkumar S, Santhiyaa RV (2018) Degradation dye using gold and silver nanoparticles synthesized by using green route and its characteristics. In: Prasad R, Jha A, Prasad K (eds) Exploring the realms of nature for nanosyn-thesis. Nanotechnology in the Life Sciences. Springer, Cham

Rana A, Kumari A, Chaudhary AK, Srivastava R, Kamil D, Vashishtha P, Sharma SN (2023) An investigation of antimicrobial activity for plant pathogens by green-synthesized silver nanoparticles using *Azadirachta indica* and *Mangifera indica*. Physchem. https://doi.org/10.3390/physchem3010010

Rastl H, Parivar K, Baharara J, Iranshahi M, Namvar F (2017) Chitin from mollusc chiton:extraction, characterization and chitosan preparation. Iran J Pharm Res 16(1):366–379

Rezazadeh NF, Buazar F, Matroodi S (2020) Synergistic effects of combinatorial chitosan and polyphenol biomolecules on enhanced antibacterial activ-ity of biofunctionalized silver nanoparticles. Sci Rep 10:19615. https://doi.org/10.1038/s41598-020-76726-7

Rinaudo M (2006) Chitin and chitosan: properties and applications. Prog Polym Sci 31(7):603–632. https://doi.org/10.1016/j.progpolymsci.2006.06.001. CODEN: PRPSB8; ISSN: 0079-6700

Saha N, Dubey VK, Bhattacharya S, Singh RK (2020) Chitosan-silver nanocom-posite: a promising antimicrobial agent. Mater Sci Eng C 110:110734. https://doi.org/10.1016/j.msec.2020.110734

Sanpui P, Murugadoss A, Prasad PD, Ghosh SS, Chattopadhyay A (2008) The antibacterial properties of a novel chitosan–Ag-nanoparticle compos-ite. Int J Food Microbiol 124(2):142–146

Sarwar A, Sohail M, Qadir MI, Naz S (2020) Chitosan-EDTA conjugate: a novel antimicrobial agent. Int J Biol Macromol 164:337–346

Sastry M, Ahmad A, Khan MI, Kumar R (2003) Biosynthesis of metal nanoparti-cles using fungi and *actinomycetes*. Curr Sci 85(2):202–206

Satapathy MK, Banerjee P, Das P (2015) Plant-mediated synthesis of silver-nanocomposite as novel effective azo dye adsorbent. Appl Nanosci 5:1–9. https://doi.org/10.1007/s13204-013-0286-x

Sayaka F, Nobuo S (2016) Water soluble EDTA-linked chitosan as a zwitterionic flocculant for pH sensitive removal of Cu(II) ion. RSC Adv 6(13):10385–10392. https://doi.org/10.1039/C5RA24175H

Sharma VK, Yngard RA, Lin Y (2009) Silver nanoparticles: green synthesis and their antimicrobial activities. Adv Colloid Interface Sci 145(2009):83–96. https://doi.org/10.1016/j.cis.2008.09.002

Shukla AK, Iravani S (2018) Green synthesis, characterization and applications of nanoparticles. Elsevier, Amsterdam

Shukla BS, Gauthier TP, Correa R, Smith L, Abbo L (2013) Treatment considera-tions in vancomycin-resistant *Enterococcal bacteremia*: daptomycin or linezolid? A review. Int J Clin Pharm 35(5):697–703

Shweta A, Raj S, Ingle AP (2019) Chitosan-based silver nanoparticles: synthesis and applications in drug delivery. Int J Biol Macromol 129:120–128

Singh V, Shrivastava A, Wahi N (2015) Biosynthesis of silver nanoparticles by plants crude extracts and their characterization using UV, XRD, TEM and EDX. Afr J Biotechnol 14:2554–2567

Singh AK (2011) X-ray diffraction: Theory and applications. Hoboken, NJ: John Wiley & Sons

Stoimenov PK, Klinger RL, Marchin GL, Klabunde KJ (2002) Metal oxide nanoparticles as bactericidal agents. Langmuir 18:6679–6686

Suryanarayana C (1998) Fundamentals of X-ray crystallography. Boston, MA: Springer Science & Business Media

Tahvilian R, Zangeneh M, Falahi H, Sadrjavadi K, Jalalvand AR, Zangeneh A (2019) Green synthesis and chemical characterization of copper nanoparticles using *Allium saralicum* leaves and assessment of their cytotoxicity, antioxidant, antimicrobial, and cutaneous wound healing properties. Appl Organometal Chem 2019:e5234. https://doi.org/10.1002/aoc.5234

Tran TH, Nguyen TT, Le TT, Nguyen TD (2019) Chitosan-coated silver nanoparticles: Synthesis, characterization, and antimicrobial activity. J Nanopart Res 21(10):1–12. https://doi.org/10.1007/s11051-019-4623-5

Tszyde M, Błońska D, Jóźwiak P, Jóźwiak M (2021) SEM-EDX analysis of heavy metals in anal papillae of *Hydropsyche angustipennis* Larvae (*Trichoptera*, Insecta) as a support for water quality assessment. https://doi.org/10.21203/rs.3.rs-150289/v1

Tufekci SK, Guzel F (2017) Influence of EDTA on the adsorption of metal ions by chitosan-based adsorbents. Environ Sci Pollut Res 24(10):9634–9644

Vanaja M, Paulkumar K, Baburaja M, Rajeshkumar S, Gnanajobitha G, Malarkodi C, Sivakavinesan M, Annadurai G (2014) Degradation of methylene blue using biologically synthesized silver nanoparticles. Bioinorg Chem Appl 2014:742346. https://doi.org/10.1155/2014/742346. Epub 2014 Mar 19. PMID: 24772055; PMCID: PMC3977556

Varadavenkatesan T, Selvaraj R, Vinayagam R (2020) Green synthesis of silver nanoparticles using *Thunbergia grandiflora* flower extract and its catalytic action in reduction of Congo red dye. Mater Today Proc 23:39–42

Verma M, Ahmad W, Park JH, Kumar V, Vlaskin MS, Vaya D, Kim H (2022) One-step functionalization of chitosan using EDTA: kinetics and isotherms modeling for multiple heavy metals adsorption and their mechanism. J Water Process Eng 49:102989. https://doi.org/10.1016/j.jwpe.2022.102989

Verstraete W, Wittebolle L, Heylen K, Vanparys B, De Vos P, Van de Wiele T, Boon N (2009) Microbial resource management: The road to go for environmental biotechnology. Eng Life Sci 9(3):285–290. https://doi.org/10.1002/elsc.200800084

Wang W, Meng Q, Li Q, Liu J, Zhou M, Jin Z, Zhao K (2020) Chitosan derivatives and their application in biomedicine. Int J Mol Sci J 21(2):487. https://doi.org/10.3390/ijms21020487. PMID:31940963;PMCID:PMC7014278

Wei S, Ching YC, Chuah CH (2020) Synthesis of chitosan aerogels as promising carriers for drug delivery: a review. Carbohyd Polym 231:115744

Yan H, Dai J, Zhang Y, Liu A, Huang X (2014) EDTA-modified chitosan: a novel adsorbent for removal of heavy metals from aqueous solutions. J Hazardous Mater Environ Chem Eng 279:384–391. https://doi.org/10.1016/j.jhazmat.2014.07.014

Zain NM, Stapley AGF, Shama G (2014) Green synthesis of silver and copper nanoparticles using ascorbic acid and chitosan for antimicrobial applications. Carbohyd Polym. https://doi.org/10.1016/j.carbpol.2014.05.081

Zhang H, Liu L, Liu W (2020a) Thermal decomposition of chitosan and its derivatives: a review. J Appl Polym Sci 137(5):48746

Zhang Y, Cao Y, Yang J, Chen X, Wang H (2020b) Chitosan-stabilized silver nanoparticles: Synthesis, characterization, and antimicrobial activity. Carbohyd Polym 247:116717. https://doi.org/10.1016/j.carbpol.2020.116717

Zulkipli M, Mahbub N, Fatima A, Wan-Lin SL, Khoo TJ, Mahboob T, Rajagopal M, Samudi C, Kathirvalu G, Abdullah NH (2022) Isolation and characterization of werneria chromene and dihydroxyacidissimol from *Burkillanthus malaccensis* (Ridl.) Swingle. Plants 11(11):1388. https://doi.org/10.3390/plants11111388

Publisher's Note